Dual diffraction bands of heliconical liquid crystal gratings

Sha Liu,[1] Hao Yu,[1] Miao Jiang,[1] Ling-Ling Ma,[2] Yan-Qing Lu,[2] and Qi-Huo Wei[1,3,*]

[1]*Department of Mechanical and Energy Engineering, Southern University of Science and Technology, Shenzhen 518055, China*

[2]*National Laboratory of Solid State Microstructures, Key Laboratory of Intelligent Optical Sensing and Manipulation, Collaborative Innovation Center of Advanced Microstructures, and College of Engineering and Applied Sciences, Nanjing University, Nanjing 210023, China*

[3]*Center for Complex Flow and Soft Matter Research, Southern University of Science and Technology, Shenzhen 518055, China*

(Received 3 March 2024; revised 8 July 2024; accepted 2 August 2024; published 15 August 2024)

Gratings composed of cholesteric liquid crystals as an important optical element for emerging applications such as augmented and virtual reality and are renowned for their characteristic single reflective diffraction band. Heliconical liquid crystal is a newly discovered state where the constituent molecules self-organize into helical structures with a non-90° polar angle between the director and the helical axis. Here, we present a numerical study on the reflective diffraction of gratings made of heliconical liquid crystals. Remarkably, numerical results demonstrate that there exist two diffraction bands at the same diffraction angle, with one peak wavelength being twice the other. We show that the short-wavelength diffraction originates from the Pancharatnam-Berry phase acquired by the reflected light while the long-wavelength diffraction stems from the reflection of the slanted volume grating, and that the wavelengths of these two diffraction bands can be attributed to the first and second band gaps of the slanted volume grating as a one-dimensional photonic crystal. We further show that the polarization of the reflected diffraction light is circular, exhibiting the same handedness as the liquid crystal for the short-wavelength band, whereas it is perfectly linearly polarized along the grating direction for the long-wavelength band.

DOI: 10.1103/PhysRevMaterials.8.085201

I. INTRODUCTION

Diffraction gratings play an important role in applications such as optical spectroscopy [1,2], flat panel displays [3], solar energy harvesting [4,5], and augmented and virtual reality [6,7]. Conventionally, these diffraction gratings manipulate the propagation phase (or the dynamic phase) of light via periodic surface profiles and can be constructed in either reflective or transmissive configurations. A growing interest lies in diffraction gratings and optical elements constructed from liquid crystal materials [8–10]. Liquid crystal optical elements present numerous advantages, including flatness, compatibility with diverse substrates, facile processing at room temperature, polarization selectivity, and close to 100% efficiency [11–17]. Such attributes render them apt for a variety of applications, ranging from lensing [11,18–22] to beam shaping [23], and extending to the realms of virtual and augmented reality [6,24,25].

Liquid crystal gratings can be broadly categorized based on optical phases that they modulate. One category relies on the Pancharatnam-Berry (PB) phase, which light acquires upon transmission or reflection [26–32]. The PB phase is typically determined by the molecular orientations in a nematic liquid crystal film for transmissive grating [23,33–36], or by the molecular orientation at the reflecting surface of a cholesteric liquid crystal for reflective grating [30–32]. The polarization state undergoes alteration upon transmission or reflection [10,37,38]. Conversely, the other category relies on a dynamic phase, which is dictated by the effective refractive indices. This category encompasses numerous tunable liquid crystal gratings where the polarization state remains constant throughout transmission or reflection [39–42]. Similarly, other optical components, including lenses and diffractive optical elements crafted from liquid crystals, can also be categorized within these two distinct classifications [43–46].

The heliconical liquid crystal, also referred to as oblique helicoidal cholesteric liquid crystal, represents a chiral nematic state initially predicted by de Gennes [47] and Meyer [48] and discovered recently in experiments by Lavrentovich *et al.* [49]. As its bend elastic constant K_3 is typically smaller than its twist elastic constant K_2 [48,50,51], the heliconical liquid crystal exhibits both the bend and twist distortions. Describing its director field necessitates two angles: the polar angle θ between the director $\boldsymbol{n}$ and the helical axis (Z axis) and the azimuthal angle φ between the director and the horizontal axis (X axis). The director $\boldsymbol{n}$ can be expressed as $\boldsymbol{n} = [\cos\varphi \sin\theta,\ \sin\varphi \sin\theta, \cos\theta]$. One remarkable feature of the heliconical liquid crystals is that the polar angle and heliconical pitch can be tuned in a wide range by applying an electric field [49,52–54], yielding intriguing electrically tunable optical properties and potential applications [55–57]. Furthermore, the heliconical liquid crystals can be engineered to respond to various external stimuli such as optical, magnetic, surface anchoring, and temperature fields [58–62] and stabilized by doping polymers [63].

*Contact author: weiqh@sustech.edu.cn

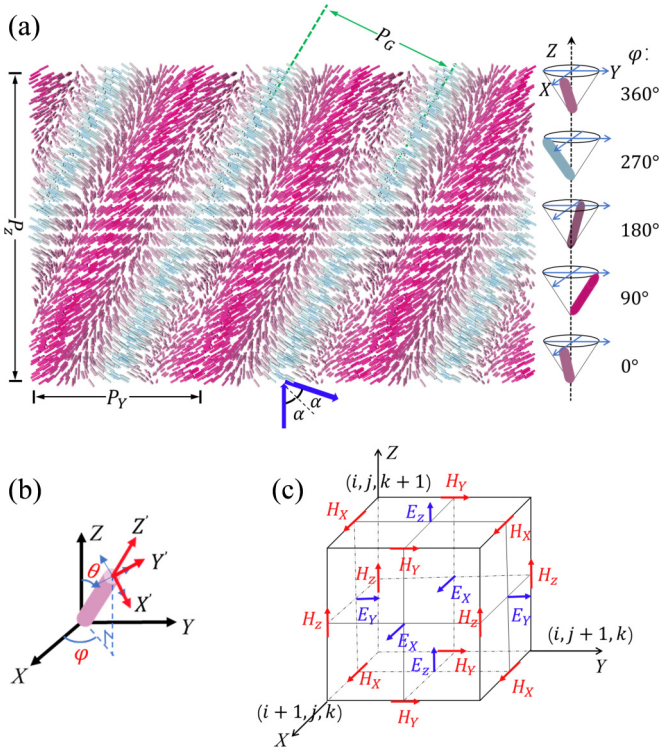

FIG. 1. (a) Schematic director field for a heliconical grating, where the bars represent local director $\boldsymbol{n}$ and the bar color represents its azimuthal angle φ. (b) The body coordinate system coincident with the principal optical axes is (X', Y', Z') and the laboratory frame coordinate system is $(X,\ Y,\ Z)$. (c) Yee discretization scheme, illustrating the lattices and components of the electric and magnetic fields.

In this paper, we present a numerical study on gratings made of heliconical liquid crystals by using a finite-difference time-domain (FDTD) method and reveal that, in contrast to only one diffraction band in cholesteric liquid crystal gratings, there are two diffraction bands with the same diffraction angle, but one band wavelength is twice that of the other. We show that the short-wavelength diffraction originates from the PB phase acquired by the reflected light that is proportional to the azimuthal angle of the molecules at the surface, and that the long-wavelength diffraction results from Bragg reflection of slanted volume gratings. The wavelengths of these two bands can be attributed to the first and second band gaps of the slanted volume grating as a one-dimensional photonic crystal. The polarization state of the diffracted light is particularly intriguing. For the short-wavelength band, the polarization of the diffracted light is circular, mirroring the handedness of the liquid crystal. However, for the long-wavelength band, the polarization of the diffracted light is linear, oriented parallel to the grating direction. These findings provide compelling insights into the optical characteristics of heliconical liquid crystal gratings, opening avenues for further exploration and potential applications.

II. NUMERICAL SIMULATION APPROACHES

Figure 1(a) depicts a heliconical liquid crystal grating, where the polar angle is θ across the material and the azimuthal angle φ is periodically altered in both the Z and Y directions. Different colors in the figure represent different azimuth angle φ. This director variation can be described by $\varphi(y, z) = 360(y/P_Y + z/P_Z)$, where P_Y and P_z represent the pitches in the Y and Z directions, respectively. These pitches denote the distances over which the liquid crystal director orientation completes a 360° rotation. It is important to note that in our assumption, the periodic grating in the Y direction does not influence the heliconical structure in the Z direction.

To describe their optical properties, we start with the Maxwell equations:

$$\nabla \times \boldsymbol{E} = -\mu_0 \frac{\partial \boldsymbol{H}}{\partial t}, \tag{1}$$

$$\nabla \times \boldsymbol{H} = \varepsilon_0 \varepsilon \frac{\partial \boldsymbol{E}}{\partial t}, \tag{2}$$

where μ_0 and ε_0 are the dielectric permittivity and magnetic permeability in vacuum, and ε is the relative dielectric permittivity. For liquid crystals, ε is a tensor that is diagonalized in the principal coordinate system (X', Y', Z') as shown in Fig. 1(b):

$$\varepsilon' = \begin{bmatrix} n_o^2 & 0 & 0 \\ 0 & n_o^2 & 0 \\ 0 & 0 & n_e^2 \end{bmatrix}, \tag{3}$$

where n_e and n_o are the extraordinary and ordinary refractive indices for polarization along and perpendicular to the local director $\boldsymbol{n}$. The relative dielectric permittivity in the laboratory frame can be obtained by two sequential rotation transformations: the first rotation transformation $\mathbf{T}_Z$ with respect to the Z axis by an angle φ and the second rotation $\mathbf{T}_Y$ with respect to the Y' axis by an angle θ, or $\varepsilon = \mathbf{T}^{-1}\varepsilon'\mathbf{T}$, where the rotation transformation matrix $\mathbf{T} = \mathbf{T}_Y\mathbf{T}_Z$. The matrix $\mathbf{T}$ can be expressed as

$$\boldsymbol{T} = \begin{bmatrix} \cos\theta\cos\varphi & \cos\theta\sin\varphi & -\sin\theta \\ -\sin\varphi & \cos\varphi & 0 \\ \sin\theta\cos\varphi & \sin\theta\sin\varphi & \cos\theta \end{bmatrix}. \tag{4}$$

We then obtain

$$\varepsilon = \begin{bmatrix} \varepsilon_{XX} & \varepsilon_{XY} & \varepsilon_{XZ} \\ \varepsilon_{YX} & \varepsilon_{YY} & \varepsilon_{YZ} \\ \varepsilon_{ZX} & \varepsilon_{ZY} & \varepsilon_{ZZ} \end{bmatrix}, \tag{5}$$

where

$$\begin{aligned}
\varepsilon_{XX} &= \left[n_o^2 - n_e^2\cos^2\theta + n_e^2 - n_o^2\right]\cos^2\varphi + n_o^2, \\
\varepsilon_{XY} &= \varepsilon_{YX} = n_e^2 - n_o^2\sin\varphi\cos\varphi\sin^2\theta, \\
\varepsilon_{XZ} &= \varepsilon_{ZX} = n_e^2 - n_o^2\cos\varphi\sin\theta\cos\theta, \\
\varepsilon_{YY} &= \left(n_e^2 - n_o^2\cos^2\varphi - n_e^2 + n_o^2\right)\cos^2\theta \\
&\quad + \left(n_o^2 - n_e^2\right)\cos^2\varphi + n_e^2, \\
\varepsilon_{YZ} &= \varepsilon_{ZY} = \sin\varphi\sin\theta\cos\theta n_e^2 - n_o^2, \\
\varepsilon_{ZZ} &= n_e^2 - n_o^2\cos^2\theta + n_o^2.
\end{aligned}$$

To calculate the optical properties of such heliconical liquid crystal gratings, we employed the FDTD method to numerically solve the Maxwell equations. The FDTD method has been established as a convenient and accurate approach for

calculating optical properties of anisotropic media like liquid crystals [33,64,65]. In this method, the space is discretized into a lattice following the Yee algorithm, as depicted in Figure 1(c). The electrical and magnetic fields are updated alternately in time steps, derived from the spatial derivatives of each other, utilizing Eqs. (1) and (2). For instance, at time step $n + 1/2$, the magnetic field can be computed from the spatial derivatives of the electrical fields, and can be expressed as follows for the X component of the magnetic field:

$$\mu_0\left[H_X^{n+\frac{1}{2}}\left(i+\frac{1}{2},j,k\right)-H_X^{n-\frac{1}{2}}\left(i+\frac{1}{2},j,k\right)\right]=\Delta t\left\{\left[E_Y^n\left(i+\frac{1}{2},j,k+\frac{1}{2}\right)-E_Y^n\left(i+\frac{1}{2},j,k-\frac{1}{2}\right)\right]\Big/\Delta Z - \left[E_Z^n\left(i+\frac{1}{2},j+\frac{1}{2},k\right)-E_Z^n\left(i+\frac{1}{2},j-\frac{1}{2},k\right)\right]\Big/\Delta Y\right\}. \quad (6)$$

At time step $n + 1$, the electrical fields are computed from the spatial derivatives of the magnetic fields from time step $n + 1/2$. As an example, the X component of the electrical field can be expressed as

$$\varepsilon_0\left[E_X^{n+1}\left(i+1,j+\tfrac{1}{2},k+\tfrac{1}{2}\right)-E_X^n\left(i+1,j+\tfrac{1}{2},k+\tfrac{1}{2}\right)\right]=\Delta t\left[\varepsilon_{XX}^{-1}H_{CX}+\varepsilon_{XY}^{-1}H_{CY}+\varepsilon_{XZ}^{-1}H_{CZ}\right], \quad (7)$$

where ε_{MN}^{-1} is the MN element of the inverse tensor ε^{-1}, H_{CM} is the M component of $\nabla \times \boldsymbol{H}$, and the subscript M and N represent X, Y, and Z. When calculating H_{CM}, interpolation using the values at neighboring grid locations is necessary. For example, H_{CY} can be approximated as

$$4\Delta Z H_{CY}=H_X^{n+\frac{1}{2}}\left(i+\tfrac{3}{2},j+1,k+1\right)+H_X^{n+\frac{1}{2}}\left(i+\tfrac{3}{2},j,k+1\right)+H_X^{n+\frac{1}{2}}\left(i+\tfrac{1}{2},j,k+1\right)+H_X^{n+\frac{1}{2}}\left(i+\tfrac{1}{2},j+1,k+1\right) - H_X^{n+\frac{1}{2}}\left(i+\tfrac{3}{2},j+1,k\right)-H_X^{n+\frac{1}{2}}\left(i+\tfrac{3}{2},j,k\right)-H_X^{n+\frac{1}{2}}\left(i+\tfrac{1}{2},j+1,k\right)-H_X^{n+\frac{1}{2}}\left(i+\tfrac{1}{2},j,k\right).$$

We exploited a commercially available FDTD algorithm (Lumerical) to solve the Maxwell equations, to take the advantage of their efficiency and reliability. Periodic boundary conditions were implemented in the X and Y directions to simulate the periodic or uniform nature of the structure. To minimize nonphysical reflections at the boundaries in the Z direction, we used perfectly matched layers at two boundaries. Perfectly matched layers are known for their effectiveness in absorbing outgoing waves, ensuring accurate simulation results.

We chose the refractive indices of the reactive mesogen RM257, with $n_e = 1.6768$ and $n_o = 1.5114$, as the parameters for our numerical computations. We conducted numerical experiments with different refractive indices and observed consistent outcomes as long as n_e and n_o are different. To minimize Fresnel reflection arising from the interface between the liquid crystal and background, we set the refractive index of the surrounding background to the mathematical average of n_e and n_o, or $n_B = 1.5941$. For all calculations, we maintain the total film thickness at $20P_Z$. A plane light wave is incident perpendicularly from a distance of $2P_Z$ to the grating surface. We verified that the numerical results converge when the mesh size is close to 10 nm or below, so we adopted 10 nm mesh size.

III. RESULTS AND DISCUSSION

Figures 2(a) and 2(b) present the calculated reflection spectra for heliconical liquid crystal gratings with the helical pitch and grating pitch fixed at $P_Z = 300$ nm and $P_Y = 1000$ nm, respectively. When the polar angle θ is 90°, the heliconical grating reverts to a conventional cholesteric LC grating, displaying a single diffraction band in the reflection spectrum [Fig. 2(a)] [6,7,66]. However, when θ is less than 90°, a second diffraction band emerges at some long wavelengths [Fig. 2(b)]. For ease of discussion, we henceforth refer to the left and right bands as the first and second bands, respectively.

The bandwidths of these two diffraction bands [67–72] exhibit complex dependence on the polar angle θ. In the case of the first band, the bandwidth exhibits a monotonical increase with the polar angle θ [Fig. 2(b)], consistent with what was observed in the heliconical liquid crystals with uniform alignment [73]. This trend can be understood by considering the effective birefringence, where the effective refractive index

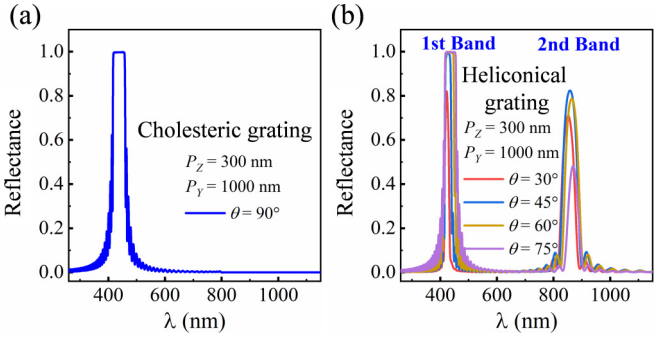

FIG. 2. Calculated reflection spectra for heliconical liquid crystal gratings with different polar angles. (a) Calculated reflection spectrum for polar angle $\theta = 90°$, or the cholesteric liquid crystal grating. (b) Calculated reflection spectra for polar angle θ ranged between 30° and 75°. The incident light is left circularly polarized and perpendicular to the grating surface. The grating pitch P_Y and the helical pitch P_Z are 1000 nm and 300 nm, respectively.

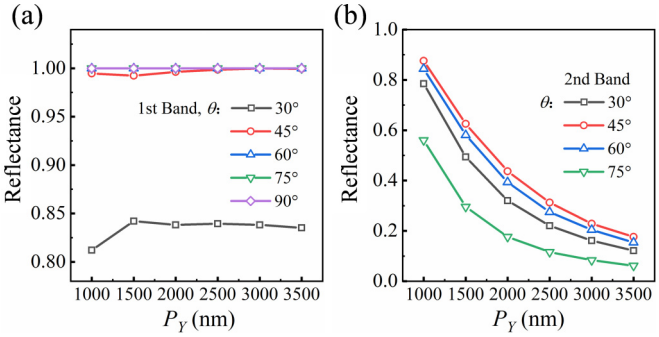

FIG. 3. Calculated reflectance for two diffraction bands. (a) Dependence of the reflectance of the first band on the grating pitch P_Y, with the helical pitch $P_Z = 330$ nm and the polar angle θ varied between 30° and 90°. (b) Dependence of the reflectance of the second band on the grating pitch P_Y, with the helical pitch $P_Z = 330$ nm and the polar angle θ varied between 30° and 75°. In all calculations, the incident light is left circularly polarized and normal to the grating surface.

can be expressed as [49,52,73]

$$n_{\text{eff}} = n_o n_e \Big/ \sqrt{n_o^2 \sin^2\theta + n_e^2 \cos^2\theta}. \tag{8}$$

It is evident that the reflection bandwidth, as determined by $(n_{\text{eff}} - n_o)P_Z$, increases with the polar angle θ. However, the width of the second diffraction band does not exhibit a visually apparent dependence on the polar angle, indicating a different underlying physical mechanism. Meanwhile, the diffraction efficiency of the first band exhibits no noticeable dependence on the polar angle unless $\theta \lesssim 30°$. In contrast, the diffraction efficiency for the second diffraction band exhibits noticeable variations with θ [Figs. 3(a) and 3(b)]: it ascends as the polar angle θ increases from 30° to 45°, and then gradually diminishes, eventually reaching zero at a polar angle of 90°.

Moreover, the diffraction efficiency displays distinct dependence on the grating pitch P_Y. For the first diffraction band [Fig. 3(a)], the intensity of diffracted light remains nearly constant regardless of the grating pitch or the diffraction angle. This behavior contrasts sharply with transmissive liquid crystal gratings based on the PB phase, where the diffraction intensity diminishes with increasing diffraction angle [33,35,74]. In contrast, for the second diffraction band, the intensity of diffracted light increases as the grating pitch decreases [Fig. 3(b)], which is contrary to the behavior observed in transmissive liquid crystal gratings. This unique characteristic of the second diffraction band renders it particularly useful in scenarios involving high diffraction angles.

We calculated their central wavelengths and plot them as functions of the grating pitch P_Y at the different polar angle θ and helical pitch P_Z (Fig. 4). Our analysis reveals that the central wavelength λ_{B1} of the first band grows monotonically with the grating pitch P_Y and the polar angle θ [Fig. 4(a)], and similarly, it grows monotonically with the helical pitch P_Z [Fig. 4(b)]. The central wavelength λ_{B2} of the second band exhibits a similar trend [Fig. 4(c)]. To elucidate the

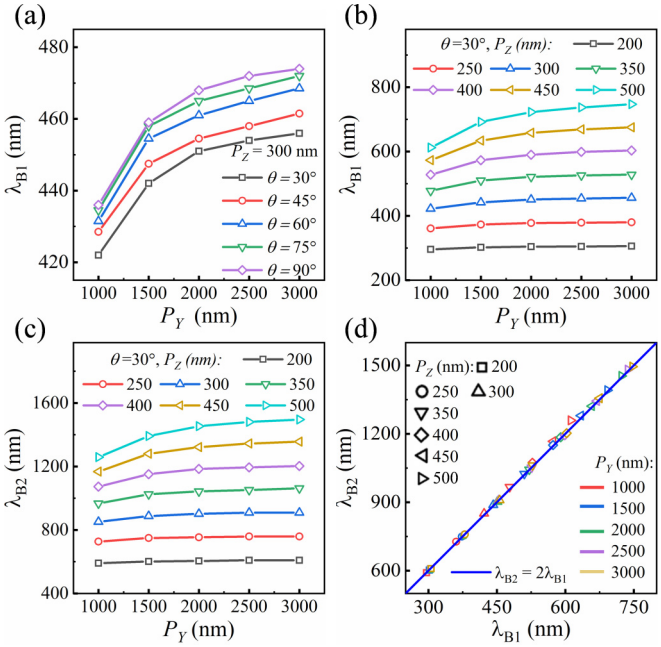

FIG. 4. Calculated central wavelengths for two diffraction bands. (a) Variations of the center wavelength λ_{B1} of the first band on the grating pitch P_Y, with the helical pitch $P_Z = 300$ nm and the polar angle θ varied between 30° and 90°. (b) Variations of the first band center wavelength λ_{B1} on the grating pitch P_Y, with fixed polar angle $\theta = 30°$ and the helical pitch P_Z varied between 200 and 500 nm. (c) Variations of the second band center wavelength λ_{B2} on the grating pitch P_Y, with the polar angle fixed at $\theta = 30°$ and the helical pitch P_Z varied between 200 and 500 nm. (d) Relationship between the center wavelengths of the dual diffraction bands. The solid line is the best fit with $\lambda_{B2} = 2\lambda_{B1}$.

relationship between the central wavelengths of these two bands, we plot λ_{B2} as a function of λ_{B1} for different grating parameters. Remarkably, we find that all data collapse into a linear master curve, which can be well fitted by the equation $\lambda_{B2} = 2\lambda_{B1}$.

We analyzed the intensity distribution of the reflected light at these central band wavelengths as a function of the reflection angle and find that most energy is diffracted into a direction not perpendicular to the surface. To quantify this observation, we determined the diffraction angle θ_B for these two bands and present a set of results for the helical pitch fixed at $P_Z = 300$ nm in Fig. 5(a) and results for the fixed polar angle $\theta = 30°$ in Fig. 5(b). We observe that for identical grating parameters and the polar angles, the diffraction angles at the central wavelengths of the first and second bands are basically identical. For the sake of convenience, we denote them as θ_{B1} and θ_{B2}, respectively.

To determine the diffraction conditions, we plot $\sin(\theta_{B1})$ and $\sin(\theta_{B2})$ versus λ/P_Y in Figs. 5(c) and 5(d), respectively, with the polar angle fixed at $\theta = 30°$. It is evident that they both follow linear relationships. By performing a best fit of the data, we find that $\sin(\theta_B) = A\lambda/P_Y$, where the prefactor $A = 1.26$ and 0.63 for the first band and the second band, respectively. Considering that the refractive index of the background materials surrounding the grating is $n_B = 1.5941$,

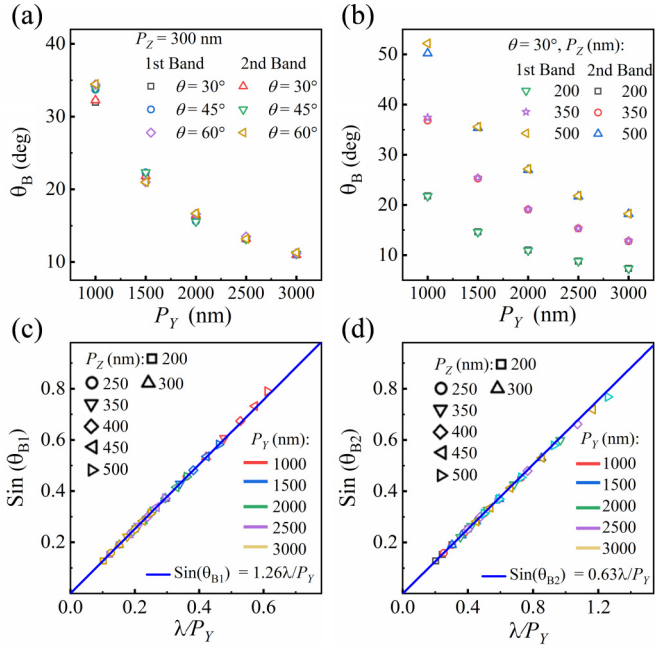

FIG. 5. Calculated diffraction angles for two diffraction bands. (a) The diffraction angles θ_B (θ_{B1} and θ_{B2}) versus the grating pitch P_Y for the helical pitch P_Z fixed at 300 nm and different polar angles θ. (b) The diffraction angles θ_B (θ_{B1} and θ_{B2}) versus the grating pitch P_Y for the polar angles θ fixed at 30° and different helical pitches P_Z. (c) $\sin(\theta_{B1})$ versus λ/P_Y for different helical pitches P_Z and grating pitches P_Y. The solid line is the best fitting with $\sin(\theta_{B1}) = 1.26\lambda/P_Y$. (d) $\sin(\theta_{B2})$ versus λ/P_Y for different helical pitches P_Z and grating pitches P_Y. The solid line is the best fitting with $\sin(\theta_{B2}) = 0.63\lambda/P_Y$.

the fitted diffraction conditions for these two bands can be rewritten as

$$n_B \sin(\theta_{B1}) = 2\lambda_{B1}/P_Y, \tag{9}$$

$$n_B \sin(\theta_{B2}) = \lambda_{B2}/P_Y, \tag{10}$$

respectively. Given that $\lambda_{B2} = 2\lambda_{B1}$, these diffraction conditions also lead to $\theta_{B1} = \theta_{B2}$, in good agreement with the numerical findings [Fig. 4(d)].

To understand the diffraction condition in Eq. (9), we revisit the reflection of circularly polarized light by cholesteric liquid crystals. The dielectric tensor of a cholesteric liquid crystal is composed of two parts: a nonperturbative one with an isotropic dielectric constant, and a perturbative one due to anisotropic modulation of the dielectric constant. The coupled-mode theory for media with periodic perturbations can yield that the reflection coefficient r can be expressed as [75]

$$r = -i\kappa \sinh sL/(s\cosh s\sqrt{2}L + i\Delta k/2 \sinh sL), \tag{11}$$

where the coupling coefficient $\kappa = \pi\alpha/n\lambda$ with $n = \sqrt{(n_e^2 + n_o^2)/2}$ and $\alpha = n(n_e - n_o)$, the wave number inside the cholesteric liquid crystal $k = \sqrt{2}\pi\sqrt{n_e^2 + n_o^2}/\lambda$, $\Delta k = 2k - 4\pi/P_z$, $s^2 = \kappa^2 - (\Delta k/2)^2$, and L is length of the helical pitch. It was shown that, with circularly polarized light with the same handedness as the liquid crystal, this reflection

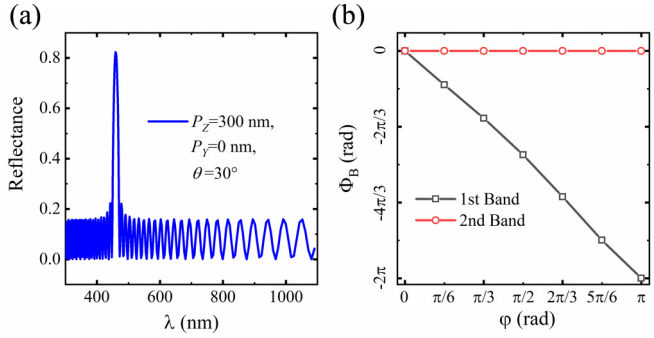

FIG. 6. Phase of the beam reflected by a uniformly aligned heliconical liquid crystal film. (a) Calculated reflection spectrum for a heliconical liquid crystal film with $P_z = 300$ nm and $\theta = 30°$. (b) Calculated phases acquired by the reflected beam upon reflection by the heliconical liquid crystal film. The square and circular data points are for wavelengths $\lambda = 460$ and 920 nm, respectively, and the solid lines represent $\Phi = -2\varphi_0$ and $\Phi = 0$, respectively.

coefficient is a complex number with a phase angle

$$\Phi = -\frac{\pi}{2} - 2\varphi(y, z = 0) - \tan^{-1}\frac{2s\cosh sL}{\Delta k \sinh sL}, \tag{12}$$

where the second term is the phase proportional to the molecular orientation at the sample surface [76]. This additional phase is present for both perpendicular and tilted illumination and can be referred to as the PB phase. The diffraction angle is determined by the generalized Snell law [21,23,77]:

$$n_B \sin\theta_B - n_B \sin\theta_{in} = \frac{\lambda}{2\pi}\frac{d\Phi}{dy}. \tag{13}$$

For normal incidence $\theta_{in} = 0$, combining Eqs. (12) and (13) gives $n_B \sin(\theta_{B1}) = 2\lambda_{B1}/P_Y$, in agreement with Eq. (9).

To further verify that the first diffraction is due to the PB phase, we did numerical calculations with heliconical liquid crystals that have uniform orientation at the surface: $\varphi(y, z) = 360z/P_Z + \varphi_0$. For vertically incident light that is circularly polarized with the same handedness as the liquid crystal, we observe only one reflection band (close to the first diffraction band of the grating) [Fig. 6(a)]. Here we used air as the background medium, so that sufficient reflectance can be obtained via Fresnel reflection at the wavelength of the second diffraction. For the wavelength within the first reflection band, the Bragg reflected light acquires an additional phase that is equal to $-2\varphi_0$ [Fig. 6(b)]. This additional phase is purely of geometric origin, and can be changed by simply rotating the heliconical liquid crystal with respect to the incident beam, similar to that in cholesteric liquid crystals [32]. This PB phase is thus a fundamental property of the heliconical liquid crystal and should be used in understanding and designing grating and reflective optical devices for the first diffraction band.

The physical mechanism for the second diffraction [i.e., Eq. (10)] is different. We observed that, for a heliconical liquid crystal with uniform surface orientation, the reflected light does not acquire any additional phase related to φ_0 [Fig. 6(b)]. As seen from the director field in Fig. 1(a), the heliconical grating forms a slanted periodic director field with an inclined angle, $\alpha = \tan^{-1}(P_Z/P_Y)$. Considering that the incident light

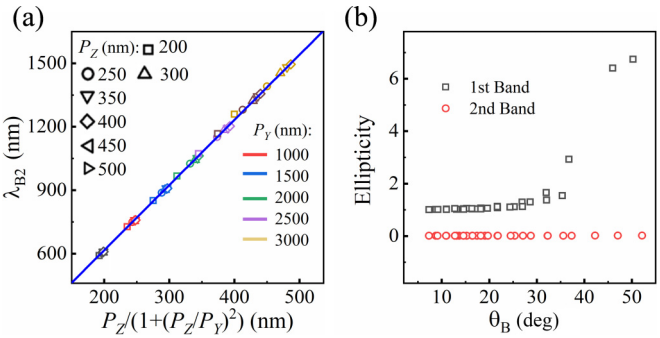

FIG. 7. (a) Calculated central wavelength of the second band as a function of the Bragg pitch P_G for different grating pitches P_Y and helical pitches P_Z. The solid line is the best fit with $\lambda_{B2} = 2\bar{n}P_z/(1 + P_Z^2/P_Y^2)$. (b) Calculated ellipticities for the diffracted beams as a function of the diffraction angle θ_B for the polar angle fixed at $\theta = 30^\circ$ and for varied grating pitch P_Y.

makes an angle α with respect to the normal of the slanted grating, the diffracted light should emerge at an angle of $\theta_{B2} = 2\alpha$.

The wavelengths of two diffraction bands are dictated by two band gaps of the one-dimensional photonic crystal, i.e., the slanted volume grating. The period (denoted as P_G) of the slanted volume grating can be related to P_Z and P_Y via a simple geometric relationship, given by [6,78]

$$P_G = P_Y P_Z/\left(P_Y^2 + P_Z^2\right)^{1/2}. \tag{14}$$

The central frequencies of the photonic band gaps for incident angle α can be expressed as $2kP_G \cos\alpha = 2\pi m$, where m are positive integers, $k = 2\pi\bar{n}/\lambda_B$, and λ_B is the wavelength in the liquid crystal medium, with $\bar{n} = (n_{\text{eff}} + n_o)/2$. The second diffraction band corresponds to $m = 1$, so we have the Bragg condition: $\lambda_{B2} = 2\bar{n}P_G \cos\alpha$. Considering Eq. (14) and $\alpha = \tan^{-1}(P_Z/P_Y)$, this Bragg condition can give the wavelength of the second band as

$$\lambda_{B2} = 2\bar{n}P_z/\left(1 + P_Z^2/P_Y^2\right). \tag{15}$$

By plotting the calculated central wavelength of the second diffraction band versus $P_z/(1 + P_Z^2/P_Y^2)$ for different P_Z and P_Y, we observe that all data collapse into a linear master curve, which can be fitted by this relation [Fig. 7(a)]. Therefore, the second band wavelength is determined by the first band gap of the one-dimensional photonic crystal of the slanted volume grating.

The first reflection band corresponds to the second band gap of the slanted volume grating, or $2kP_G \cos\alpha = 2\pi m$ with $m = 2$. This yields $\lambda_{B1} = \bar{n}P_G \cos\alpha$, which is half of λ_{B2}. Taking $\alpha = \tan^{-1}(P_Z/P_Y)$, we can obtain the wavelength of the first band:

$$\lambda_{B1} = \bar{n}P_z/\left(1 + P_Z^2/P_Y^2\right). \tag{16}$$

This is half of λ_{B2} given by Eq. (15), and thus in good agreement with the numerical results.

The diffraction conditions for these two diffraction bands are determined by the PB phase acquired by reflected light and the Bragg reflection of the slanted volume grating, respectively, and the band wavelengths are determined by the first two band gaps of the slanted volume grating as a one-dimensional photonic crystal. A recent study obtained the solutions for light propagation in heliconical liquid crystals with oblique illumination via a 4×4 matrix formalism and demonstrated in both theory and experiments the presence of multiple bands of reflections [54]. In this work, P/N are used to name these bands, where P is the heliconical pitch and N is a positive integer [54]. The first and second diffraction bands shown here for the heliconical liquid crystal gratings correspond to the $P/2$ and P bands of the slanted volume grating (i.e., $P = P_G$).

Upon further examination of the polarization states of these two diffraction bands, striking differences are observed. Figure 7(b) depicts the calculated ellipticity of these bands as a function of the diffraction angle (θ_B), with varying grating periods, while the polar angle is fixed at $\theta = 30^\circ$. For the first diffraction band, the ellipticity remains approximately 1 until the diffraction angle θ_B exceeds $\sim 30^\circ$. This suggests that the reflected light is circularly polarized for small diffraction angles and becomes elliptically polarized at higher diffraction angles.

In contrast, the ellipticity of the reflected light for the second diffraction band remains zero across all diffraction angles. This suggests that the reflected light is perfectly linearly polarized for all grating periods. Furthermore, numerical calculations demonstrate that for S-polarized incident light, the reflected diffraction beam is purely P polarized, whereas for P-polarized incident light, the polarization remains unchanged upon reflection. In other words, the heliconical grating acts as a polarization rotator for incident polarization along the grating lines but exerting no influence when the polarization is along the grating direction.

The physics behind the linear polarization seems quite complex. It has been shown that the polarization states for normal modes at the band edges of cholesteric liquid crystals are linear, but the physical pictures are nontrivial [63]. Therefore, deep understanding of the physical reason behind this linear polarization of the second diffraction band requires a rigorous theoretical model and should be an interesting topic for future study.

The identical diffraction angle of the dual bands offers advantages for integration with waveguides in augmented reality systems. This feature facilitates efficient light coupling across a broad spectrum, accommodating widely separated wavelengths [7,10]. Moreover, the polarization behavior of the second diffraction band holds promise for applications as reflective polarizers, offering the capability to switch between circular and linear polarization states.

The helical pitch of heliconical liquid crystals can be extensively tuned across a wide range of wavelengths by applying an electric field [49,52,53,73]. The grating pitch can be precisely controlled by photoalignments using two interference laser beams, in a range from micrometers to 300-nm scales. Consequently, the wavelengths of the diffraction bands, their corresponding angles, and the operational wavelength of the polarizer can all be dynamically tuned to meet specific requirements. This tunability enhances versatility and opens avenues for tailoring optical properties to achieve optimal performance in diverse applications.

IV. CONCLUSION

In conclusion, our numerical study using the FDTD method demonstrates new optical properties of gratings made of heliconical liquid crystals. The heliconical liquid crystal gratings reflect circularly polarized light with the same handedness as the helical structure at two distinct wavelength bands with one band wavelength being twice the other, and with identical diffraction angles. Notably, the diffracted light within the short-wavelength band is circularly polarized with the same handedness as the liquid crystal, while the diffracted light within the long-wavelength band is perfectly linearly polarized, consistently aligned along the grating direction.

We show that the diffraction condition for the short-wavelength bands is due to the PB phase acquired by reflected light that is proportional to the azimuthal molecular orientation angle at surface. As a contrast, the diffraction condition for the long-wavelength band is due to Bragg reflection by a slanted volume grating. The central wavelengths of the long- and short-wavelength diffraction bands are related respectively to the first and second band gaps of the slanted volume grating and are determined by the Bragg reflection conditions.

These distinctive dual diffraction bands and their unique polarization properties hold significant potential for various applications, including reflective quarter-wave plates and grating-waveguide integrated augmented reality systems.

ACKNOWLEDGMENTS

Financial support by the National Key Research and Development Program of China (Grant No. 2022YFA1405000), the National Natural Science Foundation of China (Grant No. 12174177), and by the Natural Science Foundation of Jiangsu Province, Major Project (Grant No. BK20212004) are acknowledged.

[1] D. R. Lobb, Theory of concentric designs for grating spectrometers, Appl. Opt. **33**, 2648 (1994).

[2] C. Palmer and E. G. Loewen, *Diffraction Grating Handbook* (Newport Corporation, New York, 2005).

[3] W. Wan, W. Qiao, W. Huang, M. Zhu, Z. Fang, D. Pu, Y. Ye, Y. Liu, and L. Chen, Efficient fabrication method of nanograting for 3D holographic display with full parallax views, Opt. Express **24**, 6203 (2016).

[4] J. G. Mutitu, S. Shi, C. Chen, T. Creazzo, A. Barnett, C. Honsberg, and D. W. Prather, Thin film solar cell design based on photonic crystal and diffractive grating structures, Opt. Express **16**, 15238 (2008).

[5] U. W. Paetzold, E. Moulin, D. Michaelis, W. Böttler, C. Wächter, V. Hagemann, M. Meier, R. Carius, and U. Rau, Plasmonic reflection grating back contacts for microcrystalline silicon solar cells, Appl. Phys. Lett. **99**, 181105 (2011).

[6] Y. Weng, D. Xu, Y. Zhang, X. Li, and S.-T. Wu, Polarization volume grating with high efficiency and large diffraction angle, Opt. Express **24**, 17746 (2016).

[7] Y.-H. Lee, K. Yin, and S.-T. Wu, Reflective polarization volume gratings for high efficiency waveguide-coupling augmented reality displays, Opt. Express **25**, 27008 (2017).

[8] A. Ryabchun and A. Bobrovsky, Cholesteric liquid crystal materials for tunable diffractive optics, Adv. Opt. Mater. **6**, 1800335 (2018).

[9] R. S. Zola, H. K. Bisoyi, H. Wang, A. M. Urbas, T. J. Bunning, and Q. Li, Dynamic control of light direction enabled by stimuli-responsive liquid crystal gratings, Adv. Mater. **31**, 1806172 (2019).

[10] J. Xiong and S.-T. Wu, Planar liquid crystal polarization optics for augmented reality and virtual reality: From fundamentals to applications, eLight **1**, 3 (2021).

[11] K. Gao, H.-H. Cheng, A. K. Bhowmik, and P. J. Bos, Thin-film Pancharatnam lens with low f-number and high quality, Opt. Express **23**, 26086 (2015).

[12] Y. Guo, M. Jiang, C. Peng, K. Sun, O. Yaroshchuk, O. Lavrentovich, and Q.-H. Wei, High-resolution and high-throughput plasmonic photopatterning of complex molecular orientations in liquid crystals, Adv. Mater. **28**, 2353 (2016).

[13] H. Yu, M. Jiang, Y. Guo, T. Turiv, W. Lu, V. Ray, O. D. Lavrentovich, and Q. Wei, Plasmonic metasurfaces with high UV–Vis transmittance for photopatterning of designer molecular orientations, Adv. Opt. Mater. **7**, 1900117 (2019).

[14] Y. Guo, M. Jiang, C. Peng, K. Sun, O. Yaroshchuk, O. Lavrentovich, and Q.-H. Wei, Designs of plasmonic metamasks for photopatterning molecular orientations in liquid crystals, Crystals **7**, 8 (2016).

[15] M. N. Miskiewicz and M. J. Escuti, Direct-writing of complex liquid crystal patterns, Opt. Express **22**, 12691 (2014).

[16] H. Wu, W. Hu, H. Hu, X. Lin, G. Zhu, J.-W. Choi, V. Chigrinov, and Y. Lu, Arbitrary photo-patterning in liquid crystal alignments using DMD based lithography system, Opt. Express **20**, 16684 (2012).

[17] L. De Sio, D. E. Roberts, Z. Liao, S. Nersisyan, O. Uskova, L. Wickboldt, N. Tabiryan, D. M. Steeves, and B. R. Kimball, Digital polarization holography advancing geometrical phase optics, Opt. Express **24**, 18297 (2016).

[18] M. Jiang, Y. Guo, H. Yu, Z. Zhou, T. Turiv, O. D. Lavrentovich, and Q. Wei, Low f-number diffraction-limited Pancharatnam–Berry microlenses enabled by plasmonic photopatterning of liquid crystal polymers, Adv. Mater. **31**, 1808028 (2019).

[19] Y. Li, T. Zhan, and S.-T. Wu, Flat cholesteric liquid crystal polymeric lens with low f-number, Opt. Express **28**, 5875 (2020).

[20] H. Yu, Z. Zhou, Y. Qi, X. Zhang, and Q.-H. Wei, Pancharatnam–Berry optical lenses, J. Opt. Soc. Am. B **36**, D107 (2019).

[21] Z. Zhou, Y. Guo, H. Yu, M. Jiang, T. Turiv, I. Chaganava, O. D. Lavrentovich, and Q.-H. Wei, Liquid Crystal Pancharatnam-Berry optical elements, in *Liquid Crystals XXIII*, Proceedings of SPIE Vol. 11092 (SPIE, Bellingham, WA, 2019), p. 110920D.

[22] L.-L. Ma, S.-B. Wu, W. Hu, C. Liu, P. Chen, H. Qian, Y. Wang, L. Chi, and Y. Lu, Self-assembled asymmetric microlenses for four-dimensional visual imaging, ACS Nano **13**, 13709 (2019).

[23] M. Jiang, H. Yu, X. Feng, Y. Guo, I. Chaganava, T. Turiv, O. D. Lavrentovich, and Q. Wei, Liquid crystal Pancharatnam–Berry micro-optical elements for laser beam shaping, Adv. Opt. Mater. **6**, 1800961 (2018).

[24] C. Yoo, J. Xiong, S. Moon, D. Yoo, C.-K. Lee, S.-T. Wu, and B. Lee, Foveated display system based on a doublet geometric phase lens, Opt. Express **28**, 23690 (2020).

[25] Y. Gu, Y. Weng, R. Wei, Z. Shen, C. Wang, L. Zhang, and Y. Zhang, Holographic waveguide display with large field of view and high light efficiency based on polarized volume holographic grating, IEEE Photon. J. **14**, 1 (2022).

[26] S. Pancharatnam, Generalized theory of interference, and its applications, Proc. Indian Acad. Sci. Sect. A **44**, 247 (1956).

[27] M. V. Berry, The adiabatic phase and Pancharatnam's phase for polarized light, J. Mod. Opt. **34**, 1401 (1987).

[28] P. Chen, B. Wei, W. Hu, and Y. Lu, Liquid-crystal-mediated geometric phase: From transmissive to broadband reflective planar optics, Adv. Mater. **32**, 1903665 (2020).

[29] Z. Wang, H. Zhang, X. Liu, Y. Dou, W. Duan, W. Chen, L. Ma, and Y. Lu, Cascaded liquid crystal holography for optical encryption, Chin. Opt. Lett. **21**, 120003 (2023).

[30] J. Kobashi, H. Yoshida, and M. Ozaki, Planar optics with patterned chiral liquid crystals, Nat. Photon. **10**, 389 (2016).

[31] M. Rafayelyan, G. Tkachenko, and E. Brasselet, Reflective spin-orbit geometric phase from chiral anisotropic optical media, Phys. Rev. Lett. **116**, 253902 (2016).

[32] R. Barboza, U. Bortolozzo, M. G. Clerc, and S. Residori, Berry phase of light under Bragg reflection by chiral liquid-crystal media, Phys. Rev. Lett. **117**, 053903 (2016).

[33] C. Oh and M. J. Escuti, Numerical analysis of polarization gratings using the finite-difference time-domain method, Phys. Rev. A **76**, 043815 (2007).

[34] C. Oh and M. J. Escuti, Achromatic diffraction from polarization gratings with high efficiency, Opt. Lett. **34**, 3637 (2009).

[35] K. Gao, C. McGinty, H. Payson, S. Berry, J. Vornehm, V. Finnemeyer, B. Roberts, and P. Bos, High-efficiency large-angle Pancharatnam phase deflector based on dual-twist design, Opt. Express **25**, 6283 (2017).

[36] Z. He, F. Gou, R. Chen, K. Yin, T. Zhan, and S.-T. Wu, Liquid crystal beam steering devices: Principles, recent advances, and future developments, Crystals **9**, 292 (2019).

[37] R. K. Komanduri and M. J. Escuti, High efficiency reflective liquid crystal polarization gratings, Appl. Phys. Lett. **95**, 091106 (2009).

[38] Y.-H. Lee, Z. He, and S.-T. Wu, Optical properties of reflective liquid crystal polarization volume gratings, J. Opt. Soc. Am. B **36**, D9 (2019).

[39] J. Chen, P. J. Bos, H. Vithana, and D. L. Johnson, An electro-optically controlled liquid crystal diffraction grating, Appl. Phys. Lett. **67**, 2588 (1995).

[40] C. M. Titus and P. J. Bos, Efficient, polarization-independent, reflective liquid crystal phase grating, Appl. Phys. Lett. **71**, 2239 (1997).

[41] Y. Zhang, J. Colegrove, D. B. Chung, B. Wang, and P. J. Bos, High-efficiency, liquid-crystal-based, controllable diffraction grating, J. Opt. Soc. Am. A **22**, 2510 (2005).

[42] P. F. McManamon, P. J. Bos, M. J. Escuti, J. Heikenfeld, S. Serati, H. Xie, and E. A. Watson, A review of phased array steering for narrow-band electrooptical systems, Proc. IEEE **97**, 1078 (2009).

[43] A. Jamali, D. Bryant, Y. Zhang, A. Grunnet-Jepsen, A. Bhowmik, and P. J. Bos, Design of a large aperture tunable refractive fresnel liquid crystal lens, Appl. Opt. **57**, B10 (2018).

[44] F. Chu, L.-L. Tian, R. Li, X.-Q. Gu, X.-Y. Zhou, D. Wang, and Q.-H. Wang, Adaptive nematic liquid crystal lens array with resistive layer, Liq. Cryst. **47**, 563 (2020).

[45] F. Chu, Y.-Q. Guo, Y.-X. Zhang, W. Duan, H.-L. Zhang, L.-L. Tian, L. Li, and Q.-H. Wang, Four-mode 2D/3D switchable display with a 1D/2D convertible liquid crystal lens array, Opt. Express **29**, 37464 (2021).

[46] W. Cai, Optically anisotropic, electrically tunable microlens arrays formed via single-step photopolymerization-induced phase separation in polymer/liquid-crystal composite materials, Light Adv. Manuf. **4**, 359 (2023).

[47] P. G. De Gennes, Calcul de la distorsion d'une structure cholesterique par un champ magnetique, Solid State Commun. **6**, 163 (1968).

[48] R. B. Meyer, Effects of electric and magnetic fields on the structure of cholesteric liquid crystals, Appl. Phys. Lett. **12**, 281 (1968).

[49] J. Xiang, S. V. Shiyanovskii, C. Imrie, and O. D. Lavrentovich, Electrooptic response of chiral nematic liquid crystals with oblique helicoidal director, Phys. Rev. Lett. **112**, 217801 (2014).

[50] G. Babakhanova, Z. Parsouzi, S. Paladugu, H. Wang, Y. A. Nastishin, S. V. Shiyanovskii, S. Sprunt, and O. D. Lavrentovich, Elastic and viscous properties of the nematic dimer CB7CB, Phys. Rev. E **96**, 062704 (2017).

[51] O. S. Iadlovska, K. Thapa, M. Rajabi, S. V. Shiyanovskii, and O. D. Lavrentovich, *In situ* measurements of twist and bend elastic constants in the oblique helicoidal cholesteric, Phys. Rev. E **106**, 024702 (2022).

[52] J. Xiang, Y. Li, Q. Li, D. A. Paterson, J. M. D. D. Storey, C. T. Imrie, and O. D. Lavrentovich, Electrically tunable selective reflection of light from ultraviolet to visible and infrared by heliconical cholesterics, Adv. Mater. **27**, 3014 (2015).

[53] J. Xiang, A. Varanytsia, F. Minkowski, D. A. Paterson, J. M. D. Storey, C. T. Imrie, O. D. Lavrentovich, and P. Palffy-Muhoray, Electrically tunable laser based on oblique heliconical cholesteric liquid crystal, Proc. Natl. Acad. Sci. USA **113**, 12925 (2016).

[54] O. S. Iadlovska, K. Thapa, M. Rajabi, M. Mrukiewicz, S. V. Shiyanovskii, and O. D. Lavrentovich, Electrically tunable total reflection of light by oblique helicoidal cholesteric, MRS Bull. (2024).

[55] C. Yuan, W. Huang, Z. Zheng, B. Liu, H. K. Bisoyi, Y. Li, D. Shen, Y. Lu, and Q. Li, Stimulated transformation of soft helix among helicoidal, heliconical, and their inverse helices, Sci. Adv. **5**, eaax9501 (2019).

[56] C. Xu, B. Liu, C. Peng, Q. Chen, P. Chen, P. Sun, Z. Zheng, Y. Lu, and W. Hu, Heliconical cholesterics endows spatial phase modulator with an electrically customizable working band, Adv. Opt. Mater. **10**, 2201088 (2022).

[57] B. Liu, C.-L. Yuan, H.-L. Hu, H. Wang, Y.-W. Zhu, P.-Z. Sun, Z.-Y. Li, Z.-G. Zheng, and Q. Li, Dynamically actuated soft heliconical architecture via frequency of electric fields, Nat. Commun. **13**, 2712 (2022).

[58] G. Nava, F. Ciciulla, O. S. Iadlovska, O. D. Lavrentovich, F. Simoni, and L. Lucchetti, Pitch tuning induced by optical torque in heliconical cholesteric liquid crystals, Phys. Rev. Res. **1**, 033215 (2019).

[59] S. M. Salili, Magnetically tunable selective reflection of light by heliconical cholesterics, Phys. Rev. E **94**, 042705 (2016).

[60] G. Nava, F. Ciciulla, F. Simoni, O. Iadlovska, O. D. Lavrentovich, and L. Lucchetti, Heliconical cholesteric liquid crystals as electrically tunable optical filters in notch and band-pass configurations, Liq. Cryst. **48**, 1534 (2021).

[61] O. S. Iadlovska, G. R. Maxwell, G. Babakhanova, G. H. Mehl, C. Welch, S. V. Shiyanovskii, and O. D. Lavrentovich, Tuning selective reflection of light by surface anchoring in cholesteric cells with oblique helicoidal structures, Opt. Lett. **43**, 1850 (2018).

[62] K. Thapa, O. S. Iadlovska, H. K. Bisoyi, D. A. Paterson, J. M. D. Storey, C. T. Imrie, Q. Li, S. V. Shiyanovskii, and O. D. Lavrentovich, Combined electric and photocontrol of selective light reflection at an oblique helicoidal cholesteric liquid crystal doped with azoxybenzene derivative, Phys. Rev. E **104**, 044702 (2021).

[63] M. Rumi, T. J. Bunning, and T. J. White, Polymer stabilization of cholesteric liquid crystals in the oblique helicoidal state, Soft Matter **14**, 8883 (2018).

[64] C. Oh and M. J. Escuti, Time-domain analysis of periodic anisotropic media at oblique incidence: An efficient FDTD implementation, Opt. Express **14**, 11870 (2006).

[65] H. H. Cheng, A. K. Bhowmik, and P. J. Bos, Concept for a transmissive, large angle, light steering device with high efficiency, Opt. Lett. **40**, 2080 (2015).

[66] D. Yang and S. Wu, *Fundamentals of Liquid Crystal Devices* (Wiley, New York, 2014).

[67] D. W. Berreman and T. J. Scheffer, Bragg reflection of light from single-domain cholesteric liquid-crystal films, Phys. Rev. Lett. **25**, 902 (1970).

[68] D. W. Berreman, Twisted smectic *C* phase: Unique optical properties, Mol. Cryst. Liq. Cryst. **22**, 175 (1973).

[69] M. Mrukiewicz, O. S. Iadlovska, S. V. Shiyanovskii, and O. D. Lavrentovich, Diffraction of obliquely incident light at oblique helicoidal cholesteric, in *Liquid Crystals XXVI*, edited by I. C. Khoo, Vol. 12207 (SPIE, Bellingham, WA, 2022), p. 1220709.

[70] C. Oldano, Existence of a critical tilt angle for the optical properties of chiral smectic liquid crystals, Phys. Rev. Lett. **53**, 2413 (1984).

[71] K. Hori, Angular dependence of selective reflection from the chiral smectic C phase, Mol. Cryst. Liq. Cryst. **82**, 13 (1982).

[72] K. Hori, Selective reflection of a chiral smectic C phase and a cholesteric phase, Mol. Cryst. Liq. Cryst. **100**, 75 (1983).

[73] A. Bregar, M. Štimulak, and M. Ravnik, Photonic properties of heliconical liquid crystals, Opt. Express **26**, 23265 (2018).

[74] S. Liu, H. Yu, M. Jiang, J. Feng, and Q.-H. Wei, Numerical study of transmissive liquid crystal Pancharatnam–Berry gratings with small periods, J. Opt. Soc. Am. B **40**, 431 (2023).

[75] P. Yeh and C. Gu, *Optics of Liquid Crystal Displays* (Wiley, New York, 2009).

[76] J. Kobashi, H. Yoshida, and M. Ozaki, Polychromatic optical vortex generation from patterned cholesteric liquid crystals, Phys. Rev. Lett. **116**, 253903 (2016).

[77] N. Yu, P. Genevet, M. A. Kats, F. Aieta, J.-P. Tetienne, F. Capasso, and Z. Gaburro, Light propagation with phase discontinuities: Generalized laws of reflection and refraction, Science **334**, 333 (2011).

[78] I. Nys, M. Stebryte, Y. Y. Ussembayev, J. Beeckman, and K. Neyts, Tilted chiral liquid crystal gratings for efficient large-angle diffraction, Adv. Opt. Mater. **7**, 1901364 (2019).